Process-based modeling framework for sustainable irrigation management at the regional scale: Integrating rice production, water use, and greenhouse gas emissions

Yan Bo [1, 5,6], Hao Liang [2, 5,6], Tao Li [3], Feng Zhou [1,2,4,5,4,5,*]

[1,1] Institute of Carbon Neutrality, Laboratory for Earth Surface Processes, College of Urban and Environmental Sciences, Peking University, Beijing, China.
[2,2] Jiangsu Key laboratory of Soil and Water Processes in Watershed, College of Geography and Remote Sensing, Hohai University, Nanjing, China
~~National Key Laboratory of Water Disaster Prevention, Key Laboratory of Water and Soil Processes in Watershed, College of Geography and Remote Sensing, Hohai University, Nanjing, China~~
[3] International Rice Research Institute (IRRI), Los Baños, Philippines
~~[4] College of Urban and Environmental Sciences, Peking University, Beijing, China~~
~~[5]~~ Southwest United Graduate School, Kunming, China
~~[5]~~6 These authors contributed equally

* *Correspondence to*: Feng Zhou (zhouf@pku.edu.cn)

带格式的: 非上标/ 下标
带格式的: 非上标/ 下标
带格式的: 非上标/ 下标
带格式的: 非上标/ 下标

Abstract

Rice cultivation faces multiple challenges of rising food demand while increasing water scarcity and greenhouse gas emissions, intensifying the tension of the food-water-climate nexus. Process-based modeling ~~of the nexus~~ is pivotal for developing effective measures to ~~address~~ balance these challenges. However, current models struggle to simulate their complex relationships under different water management schemes, primarily due to inadequate representation of critical physiological effects and ~~the absence of~~lack of efficient spatially explicit modeling strategies. Here, we propose an advancing framework that addresses these problems by integrating a process-based soil-crop model with vital physiological effects, a novel method for model upscaling, and the NSGA-II multi-objective optimization algorithm at a parallel computing platform. Applying the framework accounted for 52%, 60%, 37%, and 94% of the experimentally observed variations in rice yield, irrigation water use, ~~and~~ methane and nitrous oxide emissions in response to irrigation schemes. Compared with the origin model using traditional parameter upscaling methods, the advancing framework significantly reduced simulation errors by 35%−85%. Moreover, it well reproduced the multivariable synergies and tradeoffs observed in China's rice fields and identified additional 18% areas feasible for irrigation optimization, along with an additional 11% and 14% reduction potentials of water use and methane emissions, without compromising production. Over 90% of the potentials could be realized at the cost of 4% less yield increase and 25% higher nitrous oxide emissions under multiple objectives. Overall, this study provides a valuable tool for multi-objective optimization of rice irrigation schemes at a large scale. The advancing framework also has implications for other process-based modelling improvements efforts.

Key points

- This study significantly improved rice yield simulations under various irrigation schemes by ~~quantifying and~~ incorporating critical physiological processes into a process-based model.
- This study developed a novel upscaling method of model parameterization that well reproduced observed synergies and tradeoffs among multiple objectives (i.e., rice yield, irrigation water use, methane emissions, and nitrous oxide emissions).
- This study provides a practical tool for multi-objective optimization of water management to deliver co-benefits of ensuring food production, saving water, and reducing greenhouse gas emissions of rice fields.

1 Introduction

Rice is the staple food for more than half of the world's population and is also the most water-intensive cereal crop with a significant contribution to greenhouse gas emissions (GHGs) (Lampayan et al., 2015; Carlson et al., 2017). Rice cultivation currently accounts for 40% of global irrigation water use (IRR), 30% of methane (CH_4), and 11% of nitrous oxide (N_2O) emissions in agriculture (Yuan et al., 2021). To meet the demand of the growing population, a 50-60% increase in global rice production along with a 15% increase in water use are required by 2050, potentially leading to higher greenhouse gas emissions and intensifying the food-water-climate tensions of rice fields (Flörke et al., 2018). Therefore, ensuring food security while conserving water resources and reducing GHGs in rice cultivation is essential for achieving multiple United Nations Sustainable Development Goals.

Optimizing water management is promising to address the multiple challenges. However, different water management schemes can lead to a wide range of outcomes in rice yield (−16.9% to 21.9%), IRR (−68.0% to −0.3%), CH_4 (−85.5% to −0.1%) and N_2O (0% to 364%) across climatic zones, reflecting complex interactions between environmental factors and management strategies (Bo et al., 2022). Process-based models are powerful tools for predicting and managing the complicated interactions in responses to water management, given their strength in simulating crop growth, water dynamics, and soil biogeochemical processes under diverse genotype × environment × management conditions (Tian et al., 2021; Chen et al., 2022; Yan et al., 2024). Despite with several relevant studies at site-scales, extrapolation of optimized water management schemes from limited sites to the broader rice growing regions is hindered by the diverse climate, soil, crop variety, field management, etc. (Yan et al., 2024; Liang et al., 2021). Region-specific simulations of the food-water-climate nexus are thus urgently needed to identify tailored solutions. Nevertheless, current models face challenges in accurately predicting yield responses to various water management practices and adequately reproducing the spatial heterogeneity of these responses.

Despite extensive experimental research to understand critical physiological effects underlying yield responses, these processes have not been fully represented in models, especially the compensation mechanisms. Compared to continuous flooding, imposing moderate water deficit and then rewatering the field could increase both effective leaf area and net photosynthetic rate upon re-irrigation to enhance photosynthesis for biomass production (Yang and Zhang, 2010). In addition, harvest index could increase due to enhanced remobilization of assimilates and accelerated grain filling rate (Zhang et al., 2008). However, prevailing models (for example, ORYZA, DSSAT, APSIM, WHCNS) primarily focus on the negative impacts of water deficit (i.e., reduced photosynthesis or leaf rolling), while neglecting or indirectly simulating crop adaptation processes (e.g., enhanced root growth and water uptake in deeper soil layers) (Bouman et al., 2001; Li et al., 2017; Liang et al., 2021; Tsuji et al., 1998). As a

consequence, yield sensitivities to water management could be overestimated, as evidenced by evaluations of the ORYZA (v3) model (Xu et al., 2018). Moreover, physiological processes respond differently to water availability at different growth stages, while crop models generally use constant water effect coefficient throughout the rice growing season (Ishfaq et al., 2020). These imply model deficiencies in predicting yield response to water management, although no assessment across large scales exists.

Accurate model parameters are essential for reproducing spatial heterogeneity of yield, IRR, and GHGs. Previous studies usually used either the same parameters at different pixels, calibrated against all observations, or the spatial proximity principle to extrapolate model parameters for regional simulations, as a result of lacking enough observations (Zhang et al., 2024; Zhang et al., 2016). However, critical model parameters varied considerably when calibrated under different environmental and management conditions, reflecting important impact of these factors on underlying physiological and biogeochemical processes (Tan et al., 2021). As a consequence, traditional model parameterization approaches are unlikely to capture variability of yield, IRR, and GHGs due to their neglect of the environmental and management-related impacts (Song et al., 2023; Zhang et al., 2023). Besides, previous studies only evaluated simplified irrigation protocols (i.e., once drainage at midseason or alternative wetting and drying with constant threshold across the growing season) or only set bi-objectives as optimization targets (Tian et al., 2021; Chen et al., 2022), which likely underestimated the regulation potentials. Therefore, an integrated framework composed of a reliable modelling platform, broader water management schemes and multi-objective optimization targets are required for sustainable water management optimization.

To address these challenges, this study proposed an advancing framework that integrated a process-based soil-crop model (Soil Water Heat Carbon Nitrogen Simulator, WHCNS) with key physiological effects, a novel model upscaling method, and ~~the~~ a ~~NSGA-II~~ multi-objective optimization algorithm (Non-dominated Sorting Genetic Algorithm II, NSGA-II) at a parallel computing platform (see Fig.1 for workflow). This study focused on rice yield (Yield), irrigation water use (IRR), methane (CH_4), and nitrous oxide emissions (N_2O) of irrigated rice fields. First, three physiological effects were quantified and embedded into WHCNS to enhance the prediction of yield responses. Regionalized model parameters were then derived by developing parameter transfer functions for regional simulations. The model's ability to reproduce the variations in the food-water-climate nexus was extensively validated against field observations. Multi-objective optimization was conducted using the NSGA-II algorithm to investigate tradeoffs within the food-water-climate nexus and assess the regulation potentials of water management optimization. This framework was applied to China's rice cropping system as an example, considering its position as the world's largest rice producer and the ongoing conflicts between production demand, water scarcity, and greenhouse gas emissions. This study aims to provide a valuable framework for predicting and regulating rice's food-water-climate nexus towards

带格式的: 突出显示

带格式的: 突出显示

sustainable water management.

2 Data and Methods

2.1 WHCNS model and input data

The soil Water Heat Carbon Nitrogen Simulator (WHCNS) model was improved and incorporated into the advancing framework in this study to simulate rice yield, irrigation water use (IRR), methane (CH_4), and nitrous oxide (N_2O) emissions of irrigated rice fields at each pixel. The WHCNS model is a process-based agroecosystem model that runs at a daily time step and comprises six major components: surface ponding water dynamic, soil water movements, soil heat transfer, soil N transformation and transport, soil organic turnover, and crop growth. Detailed model descriptions can be found in (Liang et al., 2022; Liang et al., 2023; Liang et al., 2021). This model was chosen for several considerations: (i) the model directly outputs all four target variables simultaneously. This avoids biogeochemical models relying on crop models for detailed physiological parameters to simulate yield and calculating IRR externally to obtain all four targets as previously done (Tian et al., 2021; Yan et al., 2024), (ii) the model has been proven to simulate frequent dry-wet cycles effect reasonably well in China rice fields, due to simulating water and nitrogen dynamics in surfacing ponding water layer that is specific for rice fields (Liang et al., 2021), (iii) the model is executable at both site and regional scales with high efficiency and performs well in capturing spatial variation in key processes (Liang et al., 2023), (iv) the model has a very flexible irrigation setup, which allows for the precise control of paddy field water surface levels by setting the minimum and maximum irrigation thresholds. It also enables calculating water usage for paddy field irrigation under various water management scenarios (Jiang et al., 2021). The model is particularly suitable for simulating the regional food-water-climate nexus of rice fields.

This study ran the model at both site and regional scales (0.5-degree spatial resolution). Model input data includes daily meteorological variables, soil properties by depth, and management variables related to planting, fertilization, and irrigation (Table S1). For site-scale simulations, these variables were obtained from experimental studies, if unreported, were extracted from spatial datasets according to geographical locations. All spatial datasets were all resampled to 0.5-degree spatial resolution for regional simulations. (1) Meteorological variables, including daily mean, maximum and minimum air temperature, wind speed, precipitation, humidity, and downward solar radiation, were obtained from the fifth generation ECMWF reanalysis (ERA5) at 0.25-degree resolution (Hersbach et al., 2018). (2) Soil data including bulk density, clay contents, and soil hydraulic properties (i.e., saturated water content, field water capacity, wilting point, saturated hydraulic conductivity) at soil depths of 5, 15, 30, 60, 100, and 200 cm was obtained from SoilGrids (10 km) (Han et al., 2015). (3) The planting and harvest dates were obtained from the crop calendar data of Global Gridded Crop Model Intercomparisons (GGCMI) Phase 3 (Jägermeyr et al., 2021). (4) Fertilization practices were conducted by the auto-fertilization component of the WHCNS model, assuming

带格式的: 突出显示

带格式的: 突出显示

no nitrogen stress (Liang et al., 2023). (5) Irrigation practices are defined by three variables at daily step, including upper threshold (U_{IRR}), lower threshold (L_{IRR}, with a positive value representing field water level and a negative value representing soil water potential at 15 cm below the soil surface) and maximum allowable field water level after rainfall (H_p, also refers to as bund height). Since there is no spatially explicit information about realistic water management schemes, daily irrigation thresholds were set following Chen et al. (2022) for regional simulations. The model simulates field water level of surface ponding layer and soil water potential of stratified layers at daily step. Irrigation would be triggered whenever field water level (L_{IRR} >0) or soil water potential at 15 cm below the soil surface (L_{IRR} <0) reach the predetermined L_{IRR}. Irrigation demand is then calculated as the differences between L_{IRR} and U_{IRR}.

2.2 Compilation of experimental observations

Extensive literature reviews were conducted to collect experimental observations for model improvement and parameters calibration. Relevant studies should meet the following criteria: (1) only field experiments covering an entire growing season were included, while pot and laboratory experiments under controlled environmental conditions were excluded, (2) the control and treatments only differed concerning water management with continuous flooding (CF) as control and non-continuous flooding irrigation (NCF) as treatment, but not concerning other agronomic practices (e.g., cropping intensity, fertilizer management, and tillage). This was to isolate water management effects while avoiding confounding effects of other factors, (3) upper and lower irrigation thresholds were explicitly reported, and lower thresholds were indicated by soil water potential measured at the soil depth of 15-20 cm. Observations based on soil water potential at the other soil depth or the other soil-water indicators (e.g., soil water contents) were excluded, (4) at least one of target variables were observed, including rice yield (*Yield*), irrigation water use (*IRR*), methane emissions (CH_4), nitrous oxide emissions (N_2O), leaf area index (*LAI*), net photosynthetic rate (*Pn*), and harvest index (*HI*). For *LAI* and *Pn*, the growth stages of observations (i.e., tillering, booting, heading, and ripening stage) were recorded to account for growth stage-dependent effects. As a result, we collected observations of 119 experiments from 37 studies covering ~~29~~ 28 sites in 6 countries (i.e., China, India, Philippines, Japan, Bangladesh, and Peru) (Fig. S1). These observations were split into two datasets according to target variables. The first dataset including *Yield*, *IRR*, CH_4, or N_2O observations was used for calibration of model parameters. The second dataset of *LAI*, *Pn,* or *HI* observations was used to quantify water management effects on physiological processes for model improvement (Section 2.3).

For each paired observation under the control and treatment, the effects of non-continuous flooding irrigation were calculated as the ratio of observations under treatment to that under control (Equation 1). This yielded 251 records for R^{Yield}, 235 for R^{IRR}, 37 for R^{CH4},14 for R^{N2O}, 561 for R^{LAI} (including 61 from tillering stage, 159 from

带格式的: 字体颜色: 蓝色
带格式的: 字体颜色: 蓝色, 突出显示
带格式的: 字体颜色: 蓝色
带格式的: 字体颜色: 蓝色, 突出显示

booting stage, 202 from heading stage and 139 from ripening stage), 84 for R^{Pn} (including 42 from tillering stage, and 42 from filling stage), and 351 for R^{HI}.

$$R^X = X_{NCF} / X_{CF} \quad (1)$$

where R^X represents non-continuous flooding effects (*NCF*) on target variables X (including *Yield*, *IRR*, CH_4, N_2O, *LAI*, *Pn,* and *HI*), X_{NCF} and X_{CF} represent variable values under non-continuous flooding (*NCF*) and continuous-flooding irrigation (*CF*), respectively. Relative changes of target variables were calculated as $(R^X\text{-}1)\times100$ for interpretation and representation (e.g., $\Delta Yield$, ΔIRR, ΔCH_4, ΔN_2O).

For each paired observation, four categories of information were also collected. First, climatic variables included mean daily air temperature (*T*), precipitation (*P*), and crop evapotranspiration (*PETc*) during growing season. The difference between *P* and *PETc* was further calculated to indicate climatological water availability (*CWA*). Second, soil variables included sand content, bulk density (BD), soil organic carbon (*SOC*), pH, and soil hydrological properties (e.g., saturated water content (*SAT*), field water capacity (*FWC*)). Third, management-related variables included nitrogen application rate and timing, as well as lower (L_{AWD}) and upper (U_{AWD}) irrigation thresholds. Fourth, experimental parameters included geographical location (latitude, longitude), dates of seeding (also transplanting date in transplanted systems), anthesis, and harvest. These variables were used for running WHCNS (Section 2.1) and conducting correlation analyses (Section 3.1).

2.3 Model improvement

2.3.1 Incorporation of physiological effects

In the original WHCNS model, water management effects on crop growth were simulated by calculating water stress factor based on the Feddes reduction function (Feddes and Zaradny, 1978). Specifically, the water stress factor is calculated at daily step as a function of soil water potential to reduce root water uptake, assuming 70 kpa and 1500 kpa as thresholds of when root water uptake starts to decrease and approaches 0 (Equation 2-3). The calculated water stress factor was used to reduce the simulated actual biomass production rate, which further indirectly impact produced biomass allocated for leaf growth and yield formation (Equation 4-6).

$$T_a = \int_{L_R} S(h, h_\Phi, z)dz = T_p \int_{L_R} a_w(h, z)a_s(h_\Phi, z)b(z)dz \quad (2)$$

$$cf(w)=\frac{T_a}{T_p}=\begin{cases}\dfrac{\int_{L_R} a_w(h,z)a_s(h_\Phi,z)b(z)dz}{\omega}=\dfrac{\omega}{\omega}=1 & \omega>\omega_c \\ \dfrac{\int_{L_R} a_w(h,z)a_s(h_\Phi,z)b(z)dz}{\omega_c}=\dfrac{\omega}{\omega_c}<1 & \omega\le\omega_c\end{cases} \quad (3)$$

$$Fgc=DL\times\frac{AMAX}{K_e}\times\ln[\frac{AMAX+CC}{AMAX+CC\times(-LAI\times K_e)}] \quad (4)$$

$$Fgass=Fgc\times\frac{30}{44}\times cf(w)\times cf(N) \quad (5)$$

$$GAA(org)=Fgass\times fr(org) \quad (6)$$

where T_a and T_p are actual and potential root water uptake (cm d^{-1}). L_R indicates root length (cm). $a_w(h,z)$ and $a_s(h\Phi,z)$ are water and salt stress functions. $b(z)$ is root distribution function. w_c is the critical threshold of volumetric soil water content w above which root water uptake is reduced in water limited layers of the root zone, but the plant compensates by uptaking more water from other layers that have sufficient available water. *Fgc* is daily potential dry matter production accounting for the light interception, radiation use efficiency, and the CO_2 effects (kg hm^{-2} d^{-1}). *AMAX* is the maximum assimilation rate accounting for temperature effect (kg hm^{-2} h^{-1}). *DL*, K_e, and *CC* indicate day length (h d^{-1}), extinction coefficient (-) and actual radiation use (kg hm^{-2} h^{-1}). *Fgass* is daily actual dry matter production (kg hm^{-2} d^{-1}) accounting for water (*cf(w)*) and nitrogen stress (*cf(N)*). *GAA* indicates produced biomass allocated to organs (leaf or grains) (kg hm^{-2} d^{-1}) with the fraction of *fr(org)*.

To modify the WHCNS, NCF effects on leaf expansion, photosynthesis rate, and assimilate partition were quantified based on experimental observations and incorporated into WHCNS (Fig. ~~S1~~S2). To do so, mean values of observed effects were first calculated by experimental gradient of soil water potential (SWP, negative values) and growth stages (RDS, 0-1) (Table ~~S1~~S2-~~S3~~S4). RDS corresponds to planting, tillering, booting, heading, filling, and maturity stages was quantified as 0, 0.20, 0.40, 0.55, 0.75, and 1. Effects at other levels of SWP and RDS were then estimated by bilinear interpolation (i.e., $F^{LAI}(SWP, RDS)$, $F^{Pn}(SWP, RDS)$, $F^{HI}(SWP)$). Three functions were thus developed involving three new genetic parameters to account for differences in cultivar sensitivities (P^{LAI}, P^{Pn}, P^{HI}, Equations 7-9). The three functions were added to the origin crop growth module to modify simulations of leaf area index, net photosynthesis rate and biomass allocated into grains (Equation 10-12, Fig. 2a).

$$R^{LAI}(SWP,RDS)=1+\left[\left(F^{LAI}(SWP,RDS)\right)-1\right]\times P^{LAI} \quad (7)$$

$$R^{Pn}(SWP,RDS)=1+\left[\left(F^{Pn}(SWP,RDS)\right)-1\right]\times P^{Pn} \quad (8)$$

$$R^{HI}(SWP)=1+\left[F^{HI}(SWP)\text{-}1\right]\times P^{HI} \quad (9)$$

$$LAI'=GAA(leaf)\times SLA\times R^{LAI} \quad (10)$$

$$AMAX'=AMAX\times R^{Pn} \quad (11)$$

$$GAA(grains)'=Fgass\times fr(grains)\times R^{HI} \quad (12)$$

where R^{LAI}, R^{Pn}, R^{HI} represent NCF effects on leaf area index, net photosynthetic rate and harvest index, respectively. *SWP* represents soil water potential at 15-20 cm soil depth. *RDS* represents relative development stages (0-1). P^{LAI}, P^{Pn}, and P^{HI} are genetic parameters indicating cultivar sensitivities to irrigation regulation that were calibrated based on observations (Section 2.4). *LAI* and *SLA* are leaf area index ($m^2\ m^{-2}$) and specific leaf area ($m^2\ kg^{-1}$). *LAI'*, *AMAX'* and *GAA(grains)'* denote simulations of the modified model. It is worth noting that the three functions can be flexibly coupled to the other process-based crop models to modify the simulation of leaf area growth, biomass production, and allocation processes. The genetic parameters are needed to be recalibrated against observed yield responses considering different model structures.

2.3.2 Contribution analysis

Scenario simulations were conducted to isolate contributions of the three physiological effects on yield changes (ΔYield) (Table ~~S4~~S5). Four scenarios were simulated by considering all the three effects (S1) and omitting one of the three effects at a time (S2-S4). For each scenario, the model was run under CF and NCF conditions respectively to calculate ΔYield. The differences in the simulated ΔYield between S1 and S2-S4 represent yield changes induced by changes in leaf expansion, photosynthesis rate and assimilate partition, respectively (i.e., $\Delta Yield^{LAI}$, $\Delta Yield^{Pn}$, $\Delta Yield^{HI}$). Relative contribution of each process was calculated as the ratio of the absolute yield change induced by the process to the sum of absolute yield change induced by the three processes (Equation 13).

$$CON^{p}=\frac{\left|\Delta Yield^{p}\right|}{\sum_{p=1}^{3}\left|\Delta Yield^{p}\right|}\times 100 \quad (13)$$

where *p* represents the three new physiological processes (i.e., *p* = 1, 2, 3), CON^{p} indicates relative contribution of the process *p* to ΔYield, $\Delta Yield^{p}$ is yield changes induced by the process *p*.

2.4 Parameters regionalization

Spatially explicit model parameters are critical for reasonably reproducing spatial variabilities of target variables. In this study, seven key model parameters were selected and mapped at 0.5-degree spatial resolution due to their high influence on target variables, including accumulated temperature for crop maturity (*Cumtemp*), minimum assimilation rates (*AMIN*), the maximum CH_4 production rate per soil weight at 30 °C (*MPmax*), maximum portion of denitrification to N_2O production (f_{N2O_d}) and the three new genetic parameters (P^{LAI}, P^{Pn}, P^{HI}). These parameters were first finely calibrated at site-scales (Section 2.4.1) and then upscaled to regional scales (Section 2.4.2). To capture spatial variabilities of NCF effects, different parameters were used under CF and NCF conditions, except for genetic parameters. This was consistent with a previous modelling study, aiming to indicate different potentials of methane production and denitrification under different water management regimes (Song et al., 2023).

2.4.1 Calibration of site-scale parameters

Under CF conditions, the parameter *Cumtemp* was first determined by cultivar as the minimum cumulative daily temperature higher than 10°C (base temperature for rice growth) across all experiments using the cultivar. Then *AMIN, MPmax* and f_{N2O_d} were calibrated to achieve the best fit of predicted target variables with observations under continuous flooding conditions (i.e., experimental control). Under NCF conditions, *Cumtemp* and *AMIN* were the same with that calibrated from CF conditions. The other parameters (*MPmax*, f_{N2O_d} P^{LAI}, P^{Pn} and P^{HI}) were then calibrated by minimizing the sum of simulated squared residuals under non-continuous flooding conditions (Table ~~S5~~S6). To obtain more accurate parameter estimates, the advanced parameter estimation algorithm (PEST) was used (Doherty, 2010). As a result, 51 groups of genetic parameters (*Cumtemp*, *AMIN*, P^{LAI}, P^{Pn} and P^{HI}), 56 parameter values of *MPmax* (19 for control and 37 for treatment) and 24 parameter values of f_{N2O_d} (10 for control and 14 for treatment) were calibrated.

2.4.2 Parameters upscaling

To upscale genetic parameters (*AMIN*, *Cumtemp*, P^{LAI}, P^{Pn}, P^{HI}) calibrated at site scales to regional scales, the rice cultivar for each grid was first determined. Then, the calibrated genetic parameters of the cultivar were used to create the grid. Since the spatial distribution of rice cultivar is unknown, cultivar of each grid cell was determined as follows. First, cultivars with *Cumtemp* lower than the effective accumulative temperature requirement of the grid were identified. This ensures the cultivar could reach maturity under the grid cell's temperature conditions. The grid's temperature requirement was calculated as *Cumtemp* during rice growing periods specified by the crop calendar data of GGCMI Phase 3 (Jägermeyr et al., 2021). Subsequently, cultivars with *AMIN* that closely match the baseline *AMIN* of the grid cell were selected. The baseline *AMIN* was estimated using PEST to achieve the best

fit of yield simulation with the records in county-scale statistical yearbooks of China (downscaled to 0.5-deg spatial resolution). These procedures were designed to ensure that yield simulations were aligned with cultivar's genetic potential and spatially consistent with observations.

To upscale parameters *MPmax* and f_{N2O_d}, two parameter transfer functions (PTFs) were developed. Dependent variables were the ratio of site-calibrated parameters under treatment to that under control (i.e., R^{MPmax} and R^{fN2O_d}) (Equation 16-17). Independent variables were determined as field water capacity (*FWC*) for R^{MPmax} and bulk density (*BD*) for R^{fN2O_d}, due to their higher correlations with dependent variables. The function forms were determined as the form with the highest R^2. As a result, the relationship between field water capacity and R^{MPmax} was best fitted by an exponential function ($R^2 = 0.62$, $p < 0.001$), and the relationship between bulk density and R^{fN2O_d} was best fitted by a quadratic function ($R^2 = 0.91$, $p < 0.001$) (Fig. ~~S4~~S5). The importance of soil properties in regulating spatial heterogeneity of denitrification potentials aligns with previous studies (Tang et al., 2024). Parameters of the PTFs were calibrated using the least square method (Equation 16-17). With the calibrated PTFs, the ratio of parameters under NCF relative to CF (R^{MPmax} and R^{fN2O_d}) for each grid could be predicted by combining spatial dataset of *FWC* and *BD*. Then gridded MP_{max} and f_{N2O_d} for CF conditions (MP_{max}^{CF} and $f_{N2O\_d}^{CF}$) were estimated using PEST targeting CH_4 from the EDYGA v8.0 dataset (Crippa et al., 2024) and N_2O emissions estimated by Cui et al. (2024) (Fig. ~~S3~~S4). These parameters were estimated for 2013 and 2015 and subsequently validated for 2014 and 2016 to assess their ability to reproduce the spatial variability of target variables (Fig. ~~S2~~S3). Finally, MP_{max} *and* f_{N2O_d} for NCF conditions were calculated by multiplying MP_{max}^{CF} and $f_{N2O\_d}^{CF}$ with the predicted ratio (R^{MPmax} and R^{fN2O_d}).

$$R^{MP_{max}} = MP_{max}^{NCF} / MP_{max}^{CF} = 986 \times e^{-26 \times FWC} \quad (16)$$

$$R^{f_{N2O\_d}} = f_{N2O\_d}^{NCF} / f_{N2O\_d}^{CF} = 268 \times BD^2 + 789 \times BD + 581 \quad (17)$$

Where R^{MPmax} and R^{fN2O_d} represent the ratio of parameter *MPmax* and f_{N2O_d} calibrated under non-continuous flooding (treatment) to that under continuous flooding (control). *FWC* and *BD* represent field water capacity ($cm^3\ cm^{-3}$) and soil bulk density ($g\ cm^{-3}$) obtained from SoilGrids (10 km) (Han et al., 2015).

To prove the efficacy of the PTFs, two other parameter upscaling approaches were also used for comparison, including the mean parameters approach and the spatial proximity approach. These approaches were widely used in previous modelling studies to derive regional parameters and conduct regional simulations (Zhang et al., 2024). To adopt the mean parameter approach, mean value of the site-calibrated *MPmax* and f_{N2O_d} (Section 2.4.1) were calculated respectively for CF and NCF conditions, and then the two

constant mean parameters was used in regional simulations. To adopt the spatial proximity approach, the nearest site of a site was first identified according to geographical coordinates. Then both *MPmax* and f_{N2O_d} calibrated from the nearest site were used for simulation of this site. The three approaches were compared in their performance to reproduce the observed variations in ΔCH_4 and ΔN_2O (Fig. 3).

2.5 Regional scenario simulations and driver identification

Scenario simulations were conducted to test whether the proposed framework could reasonably predict the response sensitivity of target variables and their relations under different irrigation schemes. To do so, the well-calibrated WHCNS model was run under baseline and a series of non-continuous irrigation scenarios using the parallel computing framework (Liang et al., 2023). For baseline condition, irrigation thresholds were set according to Chen et al. (2022). For non-continuous flooding irrigation scenarios, a range of the lowest irrigation threshold levels were set based on observations (−5, −10, −15, −20, −30, −40 and −50 kpa). The upper irrigation thresholds were kept the same with baseline for consistency with experiments. NCF effects were then calculated from model simulations and compared with observed effects. Observed effects were obtained from two datasets. The first is the one compiled for this study (Section 2.2) using soil water potential to distinguish irrigation schemes. The second was obtained from Bo et al. (2022), who used the ratio of days with no surface water to total growing days (UFR) to differentiate irrigation schemes. To facilitate comparison, the UFR of each irrigation scenarios was also calculated and output by WHCNS (Fig. ~~S8~~S9).

To identify the dominant factor driving spatial patterns of NCF effects, correlation analyses between simulated NCF effects and variables were performed following (Cui et al. (, 2021). Climatic, soil and management-related factors were selected as independent variables, including T, P, ET, Clay, BD, SOC and fertilizer rate. The analyses were conducted respective for ΔYield, ΔIRR, ΔCH_4, and ΔN_2O using 3.5°-by-3.5° moving windows. The data resolution was 0.5° by 0.5°, meaning the surrounding 49 pixels were used for each grid. The correlation coefficient and its significance in each grid was first calculated, and the dominant driver was then defined as the factor with the largest absolute correlation coefficient. To assess the robustness of the results, similar analyses were done with moving windows at higher spatial resolutions (e.g., 2.5° by 2.5°).

2.6 Single-objective and multi-objective optimizations

Based on scenario simulations, four single-objectives and a multiple-objective were designed to identify optimal irrigation schemes. The four single-objective targets are (1) *maxYield*: maximizing rice yield, (2) *minIRR*: minimizing irrigation water use, (3) *minCH_4*: minimizing CH_4 emission, and (4) *minN_2O*: minimizing N_2O emissions. Under all targets, yield reduction compared to CF conditions was avoided. With optimal

带格式的: 突出显示
带格式的: 突出显示
带格式的: 突出显示
带格式的: 字体颜色: 自动设置, 突出显示
带格式的: 突出显示
带格式的: 突出显示
带格式的: 突出显示
带格式的: 突出显示
带格式的: 突出显示
带格式的: 突出显示
带格式的: 突出显示
带格式的: 字体: 非倾斜, 突出显示
带格式的: 突出显示
带格式的: 字体: 非倾斜, 突出显示
带格式的: 突出显示
带格式的: 字体: 非倾斜, 突出显示
带格式的: 字体: 非倾斜, 突出显示
带格式的: 突出显示
带格式的: 字体: 非倾斜, 突出显示
带格式的: 突出显示
带格式的: 突出显示
带格式的: 突出显示
带格式的: 突出显示
带格式的: 突出显示
带格式的: 突出显示
带格式的: 突出显示
带格式的: 突出显示
带格式的: 突出显示
带格式的: 突出显示
带格式的: 突出显示
带格式的: 突出显示
带格式的: 突出显示
带格式的: 突出显示
带格式的: 突出显示
带格式的: 突出显示
带格式的: 突出显示
带格式的: 突出显示
带格式的: 突出显示
带格式的: 突出显示
带格式的: 突出显示
带格式的: 突出显示
带格式的: 突出显示
带格式的: 突出显示
带格式的: 突出显示

solution under the four single-objective scenarios, the largest regulation potentials to increase yield and reduce IRR, CH_4, and N_2O emissions were assessed. For comparison, the scenario simulations and optimization were also conducted using the origin WHCNS model (Fig. 5).

The multi-objective optimization was conducted by combining the improved WHCNS model and the NSGA-II algorithm (Deb et al., 2002). First, a set of 100 parental populations was initialized with random solutions. Each population includes 1993 individuals, corresponding to 1993 grid cells of irrigated rice areas. Second, the objective functions were computed with each solution by executing the WHCNS model (Equation 18). Third, the performance of each population was evaluated by ranking the fitness of its objective functions. Fitness is a measure of how well a solution performs and is calculated based on the non-dominated sorting rank. Then, a new generation was generated through selection, crossover, and mutation based on fitness. Finally, Pareto fronts were generated after 100 generations had been evaluated (that is 10000 populations).

带格式的: 突出显示

$$f_{objective} = \begin{bmatrix} f_{max}\{\sum_{n=1}^{N} WHCNS(yield)\} \\ f_{\min}\{\sum_{n=1}^{N} WHCNS(IRR)\} \\ f_{\min}\{\sum_{n=1}^{N} WHCNS(GWP)\} \end{bmatrix} \quad (18)$$

$$WHCNS(GWP) = 27.2 \times WHCNS(CH_4) + 273 \times WHCNS(N_2O) \quad (19)$$

where $f_{objective}(yield, IRR, GWP)$ denotes the collection of objective functions, f_{max} denotes the objective that needs to be maximized (e.g., rice yield), and f_{min} denotes the objective that needs to be minimized (e.g., IRR, GWP). GWP is the integrated global warming potential of combined emissions of CH_4 and N_2O emissions and is calculated based on WHCNS simulations (Equation 19) (Forster et al., 2021). It should be noted that this study set equal weight for each target variable to evaluate the fitness of each solution. Decision-makers can simply set the weight values of different objectives according to their preferences, or adopt advanced multi-objective criteria decision-making methods such as the efficiency coefficient method (Guo et al., 2021). The regulation potentials of multiple-objective optimization were calculated as the averaged NCF effects (ΔYield, ΔIRR, ΔCH_4, ΔN_2O, ΔGWP) of all non-dominated solutions. The potentials were further compared with that from single-objective optimizations to investigate tradeoffs between target variables (Fig. 6).

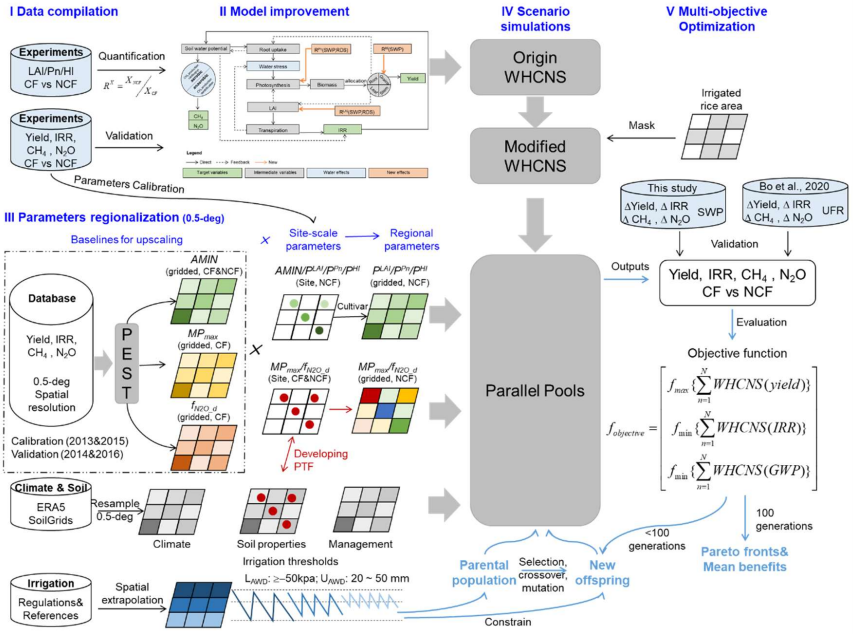

Figure 1 Research framework of this study. The framework mainly combines *data compilation*, *model improvement*, *parameter regionalization, scenario simulations, and multi-objective optimization*. The framework can be flexibly adapted with alternative irrigation scenarios, optimization objectives, and optimization algorithms in other modelling studies. *LAI*, *Pn*, and *HI* represent leaf area index, net photosynthetic rate, and harvest index. *AMIN*, *MPmax*, f_{N2O_d}, P^{LAI}, P^{Pn}, and P^{HI} are model parameters calibrated and mapped in this study (Section 2.4). *CF* and *NCF* represent continuous flooding and non-continuous flooding irrigation. *SWP* and *UFR* represent soil water potential and the ratio of unflooded days to total rice growing days, indicating different irrigation schemes. See the *Appendix* for detailed descriptions of parameters and variables.

3 Results and discussion

3.1 Performance of model improvement

The origin WHCNS model was first evaluated in reproducing variabilities of rice yield and irrigation water use under various irrigation schemes. For rice yield, model performance is satisfying when mixing observations under continuous flooding (CF, experimental control) and non-continuous flooding (NCF, experimental treatments) irrigation schemes together (R^2 = 0.41, normalized root mean square error *nRMSE* = 11%) (Fig. ~~S5~~S6). In particular, with fine-turned crop genetic parameters (i.e., *Cumtemp* and *AMIN*), the origin model performed well under CF condition (R^2 = 0.74, *nRMSE* = 1 3%), while had worse performance under NCF condition (R^2 = 0.22, *nRMSE* = 13%)

(Fig. ~~S5~~S6). As a consequence, the origin model failed to reproduce variations in observed yield changes (ΔYield) (R^2 = 0.03, *nRMSE* = 17%) (Fig. 2b). More importantly, the simulations could not reproduce ΔYield sensitivities to soil water potentials presented in field experiments (Fig. 2d). In contrast to yield, model performance in simulating irrigation water use responses (ΔIRR) variabilities and its sensitivities to soil water potentials was acceptable (Fig. 2c and 2e). These results highlight the primary modelling deficiency in simulating ΔYield. Given the satisfying model performance in simulating yield under CF and ΔIRR, the underperformance is likely due to lacking critical physiological processes responsible for yield responses to NCF rather than uncertainties of crop parameters.

After incorporating the three functions of NCF effects and fine calibration of genetic parameters (Section 2.3, Fig. 2a), the model performance was substantially improved. The explained variabilities of ΔYield increased from 3% to 52% and *nRMSE* decreased from 17 % to 11% (Fig. 2b). The observed ΔYield sensitivities to soil water potential (9% kpa^{-1}, $P < 0.001$) could be reasonably reproduced by the modified model (13% kpa^{-1}, $P < 0.001$) rather than the origin mdoel ($P > 0.05$) (Fig. 2d). The cultivar differences of yield responses could also be simulated (R = 0.67) (Fig. ~~S6~~S7). Across the three processes, leaf area growth ($\Delta Yield^{LAI}$) was primarily responsible for yield losses, while net photosynthetic rate ($\Delta Yield^{Pn}$) and biomass translocation ($\Delta Yield^{HI}$) contributed to yield increases (Section 2.3.2, Fig. ~~S7~~S8). The positive contributions are larger in warmer and more humid areas, and in acidic soils with larger field water holding capacity and higher SOC. These findings conform with empirical relationships between ΔYield and environmental factors reported by previous meta-analysis (Carrijo et al., 2017). These results prove efficacy of the modified model to predict and regulate ΔYield under diverse irrigation schemes and environmental conditions.

~~Besides being coupled to WHCNS as an integrated system, the new functions also contribute to advancing related modelling studies by directly involving positive physiological effects and considering stage-dependent response sensitivities (Li et al., 2017). By contrast, most prevailing crop models only account for negative effects of soil drying and reduced transpiration, while does not incorporating direct compensation effects (such as increased photosynthesis rate upon rewatering) . Moreover, constant stress sensitivity parameters were generally used for all growth stages (such as ORYZA and DSSAT) (Bouman et al., 2001; Tsuji et al., 1998). These models could flexibly incorporate the three new functions and recalibrate the genetic parameters (i.e., P^{LAI}, P^{Pn}, and P^{HI}) following the procedures of this study to improve their performance in predicting yield responses.~~

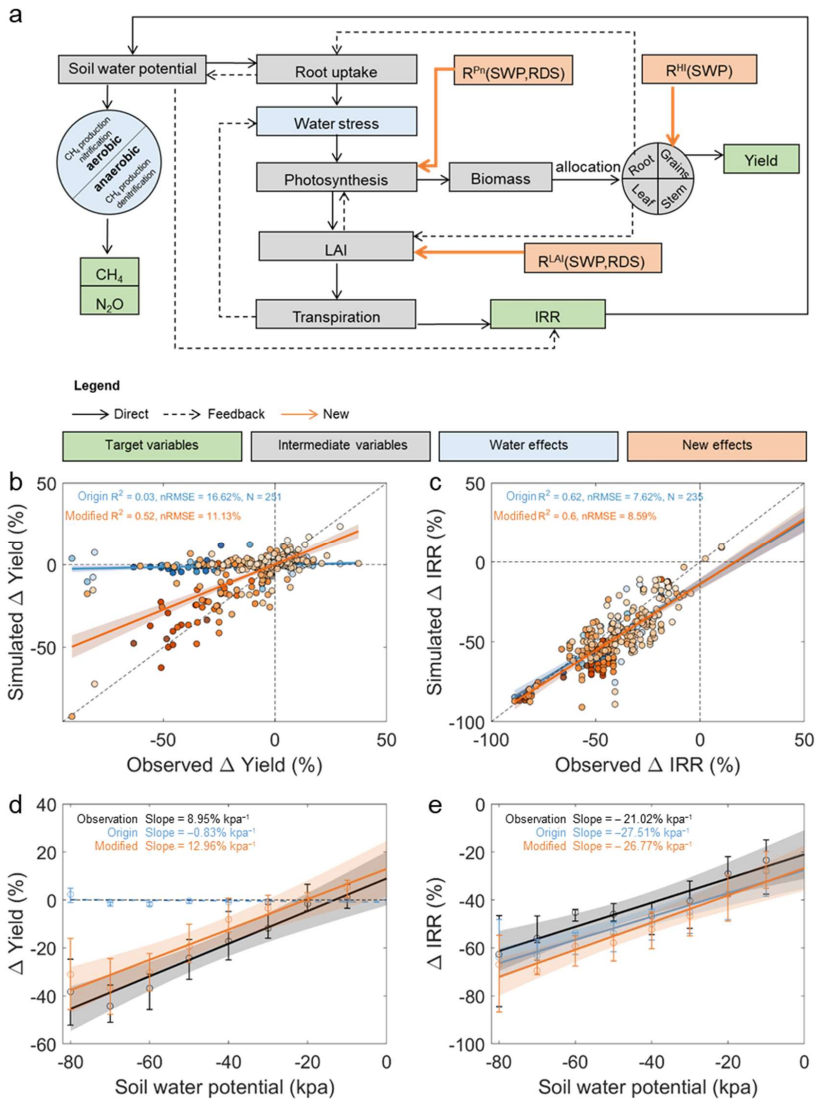

Figure 2 Model improvements by incorporating water effects on physiological processes. (a) Schematic of critical physiological effects in response to different irrigation schemes and their representation in the WHCNS model. **(b-c)** Model performance for simulating ΔYield **(b)** and ΔIRR **(c)** based on the origin (blue) and modified (orange) WHCNS model. Darker colored dots indicate lower soil water potential (unit: kpa). **(d-e)** Sensitivity of ΔYield and ΔIRR to lower irrigation threshold of soil water potential. Black, blue, and orange colors show the results of observations and simulations based on the origin and modified WHCNS model, respectively. Circles

are mean values; error bars show the 25–75% interquartile range. The lines are the linear regression lines with dashed lines indicating non-significant relationships based on two-sided t-test (P > 0.05). The shaded areas around each line represent the 95% confidence interval.

Besides being coupled to WHCNS as an integrated system, the new functions also contribute to advancing related modelling studies by directly involving positive physiological effects and considering stage-dependent response sensitivities (Li et al., 2017). By contrast, most prevailing crop models only account for negative effects of soil drying and reduced transpiration, while does not incorporating direct compensation effects (such as increased photosynthesis rate upon rewatering) . Moreover, constant stress sensitivity parameters were generally used for all growth stages (such as ORYZA and DSSAT) (Bouman et al., 2001; Tsuji et al., 1998). These models could flexibly incorporate the three new functions and recalibrate the genetic parameters (i.e., P^{LAI}, $P^{Pn,}$ and P^{HI}) following the procedures of this study to improve their performance in predicting yield responses.

3.2 Performance of regionalized parameters

To simulate regional NCF effects, the model was first run respectively for CF (baseline) and NCF conditions using the parallel computing framework at a spatial resolution of 0.5-deg. NCF effects were then calculated using model simulations following Equation 1 (Fig.1 and Section 2.4). Using the PEST-calibrated gridded model parameters for CF (Section 2.4.1), the *nRMSE* between model simulations and their spatial datasets were 20% to 29% for yield, ~7% for IRR, ~4% for CH_4, and 4% to 6% for N_2O during the validation period (year 2014 and 2016) (Fig.S2). It was noted that the *nRMSE* of rice yield was relatively larger than that of other target variables, despite being within an acceptable range (<30% for the validation periods). This could be caused by interannual cultivar changes, which was difficult to consider in large-scale simulations due to the lack of spatial distribution of rice cultivars. Overall, these results reveal a satisfying model calibration to simulate baseline values and spatial variabilities of target variables.

To reproduce observed variabilities of NCF effects on target variables, NCF effects on key model parameters (*MPmax* and f_{N2O_d}) were incorporated for constraining model simulations. To do so, NCF effects on model parameters were first quantified from site-scale calibrations and extrapolated to regional scale (Section 2.4). Three approaches of parameter extrapolation were tested and compared, including developing parameter transfer functions (PTFs), using mean site-calibrated parameters (mean), and using spatially nearest calibrated parameters (spatial) (Section 2.4.3). Results showed that developing PTFs performed the best to reproduce observed variabilities of ΔCH_4 and ΔN_2O (Fig. 3). Model simulations using parameters estimated by PTFs explained 37% and 94% of variations in ΔCH_4 and ΔN_2O, with *nRMSE* being 25% for ΔCH_4 and 10% for ΔN_2O (Fig. 3a-b). By contrast, simulations based on the other two approaches could hardly reproduce observed variabilities of ΔCH_4 and ΔN_2O, with *nRMSE* achieving 66%

to 72% for ΔCH_4 and 29% to 73% for ΔN_2O (Fig. 3c-f). These results prove the efficacy of the developed PTFs and suggest soil variables as good predictors for spatial extrapolation of site-calibrated parameters to simulate CH_4 and N_2O. The PTFs could also be referred by other biogeochemical models for regional simulations of CH_4 and N_2O (such as the Denitrification-Decomposition model ~~DNDC~~ and the Dynamic Land Ecosystem Model~~DLEM~~) (Zhang et al., 2016).

带格式的: 突出显示

带格式的: 突出显示

带格式的: 突出显示

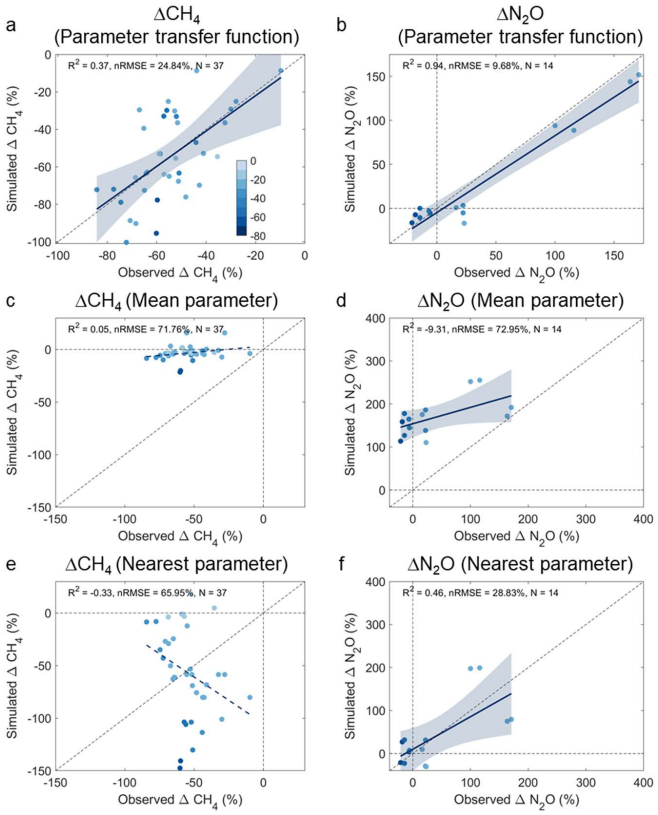

Figure 3 Comparison of model parameter upscaling approaches. Model performance in simulating methane and nitrous oxide emissions changes based on parameters derived from **(a-b)** parameter transfer functions (PTFs), **(c-d)** mean site-calibrated parameters, and **(e-f)** spatially nearest parameters. The color of the dots indicates lower irrigation thresholds of soil water potential under non-continuous flooding irrigation (unit: kpa). The solid lines are regression lines with dashed lines indicating non-significant relationships ($P > 0.05$). Blue shading around each line represents the 95% confidence interval.

Considering scarce observations of NCF effects across space, it was impractical to directly evaluate the regionalized parameters in reproducing spatial~~tial~~

~~vatiability~~variability of NCF effects. Therefore, the proposed framework was evaluated in terms of the response sensitivity of target variables and their relationships under different irrigation schemes (Section 2.5). Scenario simulations broadly conformed with observations regarding the magnitude of NCF effects and response sensitivity across soil water potential gradients (Fig. ~~S8~~S9). With decreased soil water potential threshold, ΔYield decreased quasi-linearly, ΔCH_4 and ΔIRR decreased at a decelerating rate, while ΔN_2O showed slight variabilities (Fig. ~~S8a~~S9a). The decelerating decrease in ΔCH_4 was also observed in experiments, suggesting the model ability to simulate maximum potentials of CH_4 mitigation (Balaine et al., 2019). The response sensitivity was further validated using an alternative observation dataset (Fig. ~~S8b~~S9b). Besides, the observed synergy or tradeoffs of the yield-IRR-GHGs nexus were broadly covered by scenario simulations using the modified model rather than using the origin model (Fig. ~~S8c~~S9c). Such bias could further impact assessment of regulation potentials of the food-water-climate nexus.

3.3 Assessment of regional regulation potentials

Scenario simulations revealed large spatial variabilities of NCF effects on all target variables (Fig. 4). Applying the ~~the~~ same irrigation scheme (e.g., lower irrigation threshold of −15 or −30 kpa) could induce larger yield increase in the southwest single-rice region~~s~~ (XNS: 2.4% to 3.4%), while larger yield losses in northern regions (HHH: −3.2%) (Fig. 4a and b). The HHH region also showed larger yield sensitivity~~–~~ with decreased lower irrigation threshold (−0.24% kpa^{-1}) (Fig. 4c). For IRR, relatively larger water saving benefits occurred in south regions, whereas response sensitivity was larger in northeast regions (−1.7% kpa^{-1}). For CH_4, north rice growing regions showed relatively higher reductions (NES: 64% to 82%, HHH: 77% to 88%) and higher response sensitivity to decreased soil water potential threshold. The findings about larger water saving benefits in south China and larger CH_4 mitigation in north China were consistent with previous assessments (Tian et al., 2021). However, N_2O emissions showed widespread increase regardless of lower irrigation threshold, except for northeast regions, indicating low opportunities to reduce N_2O by only optimizing water management.

To further understand the drivers shaping the spatial variations in NCF effects, correlation analyses were conducted for each target variable across varying lower irrigation threshold. Overall, climatic and edaphic variables were the most important drivers, while management-related variables were less important (Fig. 5). Exceptions occurred in the south double rice region (HND) for ΔYield and the southwest single rice region (XNS) for ΔN_2O, where higher fertilizer application rate was associated with larger yield increase but decreased N_2O reduction potentials (Fig. S10 and S11). For both ΔYield and ΔIRR, clay content was the most important driver at higher irrigation thresholds, while climate factors showed increasing importance with decreased irrigation thresholds (Fig. 5a and b). By contrast, reduction potentials for

带格式的: 突出显示
带格式的: 突出显示
带格式的: 突出显示
带格式的: 突出显示
带格式的: 突出显示
带格式的: 字体颜色: 蓝色, 突出显示
带格式的: 字体颜色: 蓝色
带格式的: 字体颜色: 蓝色, 突出显示
带格式的: 突出显示
带格式的: 突出显示
带格式的: 突出显示
带格式的: 突出显示
带格式的: 突出显示
带格式的: 突出显示
带格式的: 突出显示
带格式的: 突出显示
带格式的: 下标, 突出显示
带格式的: 突出显示
带格式的: 突出显示
带格式的: 突出显示
带格式的: 突出显示
带格式的: 突出显示
带格式的: 突出显示
带格式的: 突出显示
带格式的: 突出显示
带格式的: 突出显示
带格式的: 突出显示

CH_4 and N_2O emissions were dominated by edaphic factors regardless of irrigation threshold (i.e., clay for CH_4 and bulk density for N_2O) (Fig. 5c and d). These findings highlight the complex interplay of factors influencing regulation potentials of rice production, irrigation water use and greenhouse gas emissions through NCF adoption.

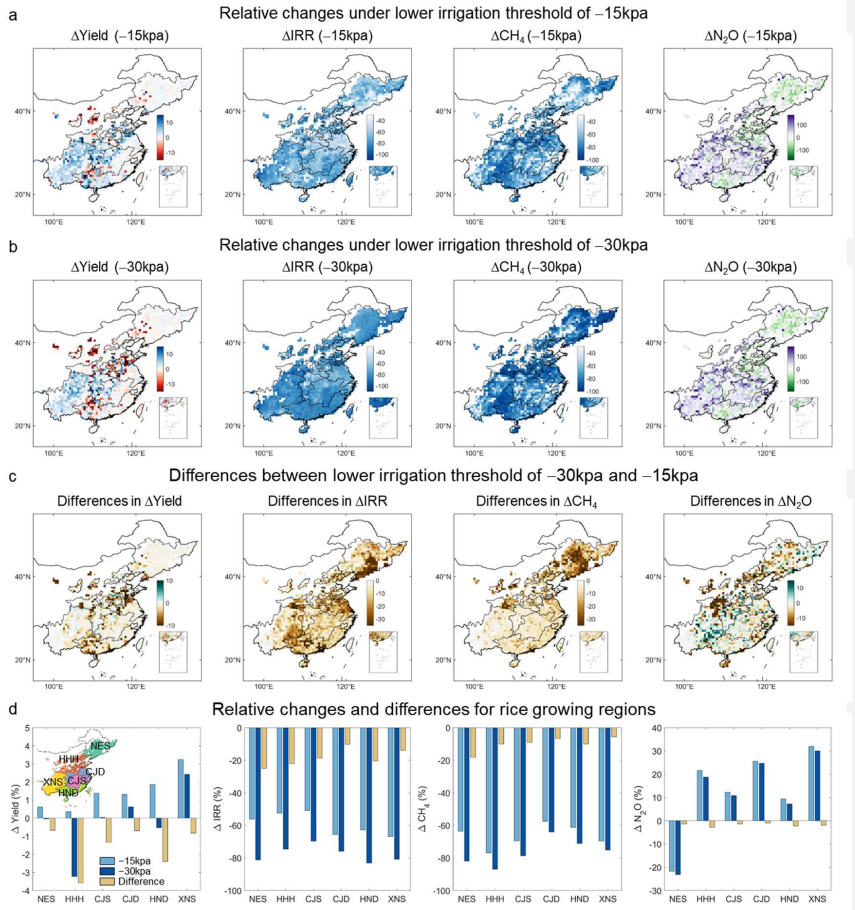

带格式的: 突出显示
带格式的: 下标
带格式的: 突出显示
带格式的: 突出显示

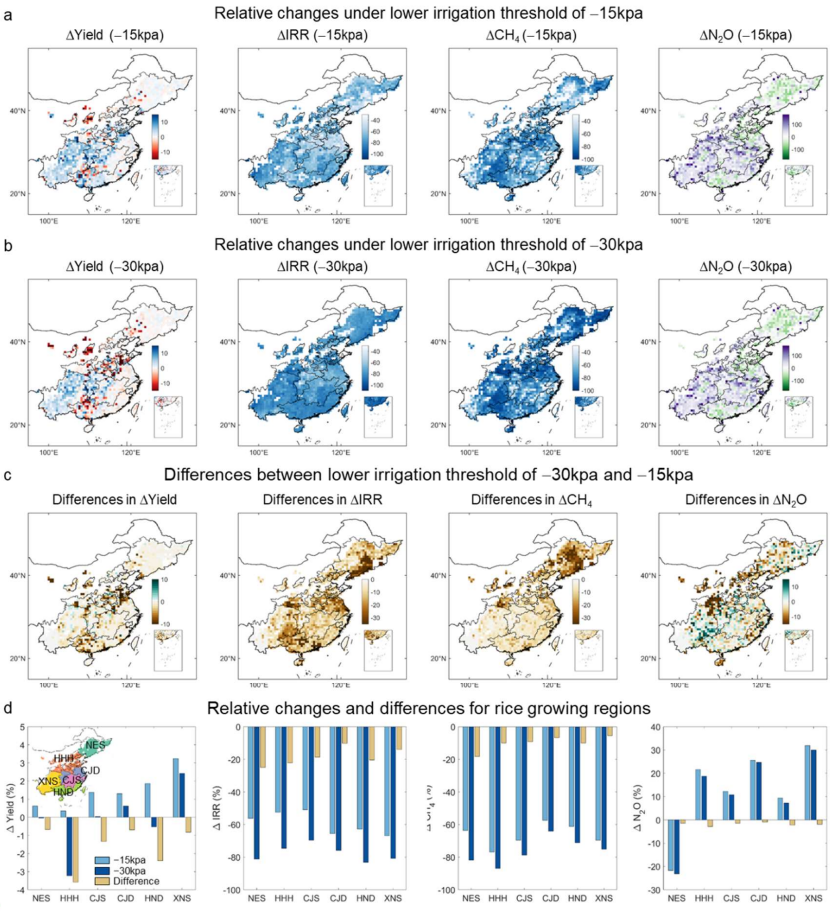

683 —

684 **Figure 4 Spatial pattern of relative changes in target variables under different**
685 **irrigation schemes ~~and differences~~.** The four columns correspond to the four target
686 variables ΔYield, ΔIRR, ΔCH_4, and ΔN_2O, respectively. **(a)** relative changes of target
687 variables under a lower irrigation potential of −15 kpa, **(b~~a~~)** relative changes of target
688 variables under a lower irrigation potential of −30 kpa, **(c)** differences between (b) and
689 (a), **(d)** results for different rice growing regions. NES, HHH, CJS, CJD, HND, and
690 XNS indicate six rice growing areas of China, namely, Northeast Single rice,
691 HuangHuaiHai single rice, Yangtze River single rice, Yangtze River double Rice, South
692 China Double rice, and Southwest China Single rice, respectively.
693
694

带格式的: 两端对齐

带格式的: 两端对齐

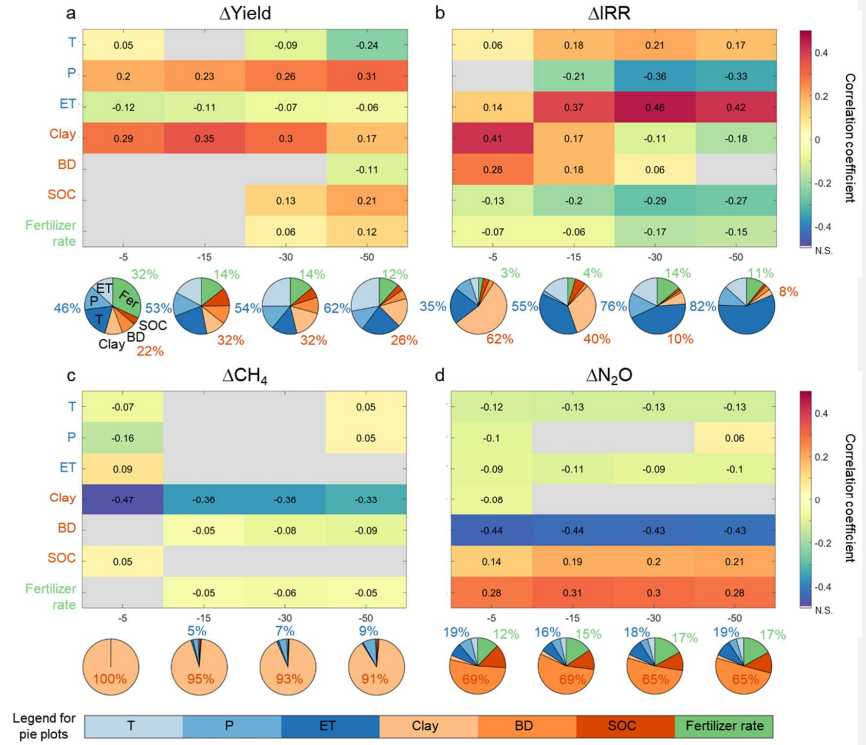

Figure 5 Drivers regulating spatial variations in relative changes in yield (a), IRR (b), CH_4 (c) and N_2O (d). The numbers and colors indicate correlation coefficients, with gray indicating non-significant correlations (N.S., $P \geq 0.05$). The pie plots represent the proportion of irrigated rice areas (%) for which relative changes variation is regulated by the dominant drivers. The dominant driver is defined as the factor with the largest absolute correlation coefficient in each grid cell, identified from 3.5°-by-3.5° moving windows. The numbers in blue, orange and green around the pie plots denote the area proportions dominated by climate (i.e., T + P + ET), soil (i.e., Clay + BD + SOC) and management-related (i.e., Fertilizer rate) factors under corresponding lower irrigation threshold. Spatial distributions of dominant drivers are shown in Fig. S10 and S11.

~~Four single objective targets were designed~~ ~~T~~to identify the largest regulation potentials from NCF adoption, four single objective targets were designed, including maximizing rice yield, minimizing IRR, CH_4 emissions, or N_2O emissions (denoted as *maxYield, minIRR, minCH_4, min N_2O,* Section 2.6). Results indicated that the largest regulation potentials of ΔYield, ΔIRR, ΔCH_4 and ΔN_2O were 4.6%, −61.0%, −64.2% and −10.9%, respectively (Fig. ~~5a~~6a). These potentials could be achieved respectively

带格式的: 字体: 非加粗
带格式的: 字体: 非加粗
带格式的: 字体: 非加粗
带格式的: 字体: 非加粗

over 91%, 91%, 88% and 26% of national rice areas (Fig. ~~5b~~6b). Spatially, larger yield increase potential occurred in south (HND: 7.7%) and southwest regions (XNS: 6.8%) (Fig. ~~S9A~~S12A). The reduction potential of IRR and CH_4 showed relatively slight spatial variabilities. In contrast, reduction potential of N_2O primarily concentrated in northern regions (NES: −30%) due to increased N_2O in southern regions (Fig. 5a and ~~S9A~~S12A). N_2O increase in southern regions is associated with higher nitrogen application rates, providing substrate for nitrification and denitrification processes to facilitate N_2O emissions (Jiang et al., 2019). The results conform to previous studies in that irrigation and nitrogen should be co-regulated for these areas to avoid unintended N_2O emissions from water management (Jiang et al., 2019; Kritee et al., 2018).

The largest regulation potentials of ΔYield, ΔIRR, ΔCH_4, and ΔN_2O are not likely to be achieved at the same time, as evidenced by different optimized irrigation strategies between single-objective targets (Fig. ~~5~~ 6 and ~~S10~~S13). For example, the lower irrigation threshold should be higher than −20kpa for most areas (84%) under *maxYield*, while lower than −20kpa over half areas under *minIRR* and *minCH_4*. This suggests tradeoffs between yield increase and IRR/CH_4 mitigation (Bo et al., 2021). To compare, using the origin model could overlook nearly 20% feasible areas for applying optimized irrigation schemes (Fig. ~~5~~6). As a consequence, regulation potentials of ΔYield, ΔIRR, ΔCH_4 and ΔN_2O could be underestimated by 4%, 11%, 14%, and 2%, especially for the southwest regions (XNS) (Fig. ~~5a~~6a). Moreover, optimal NCF strategies also differed from that identified by the improved model, particular under *maxYield* targets (Fig. ~~5b~~6b). These results showed important implications of the improved framework for prompting sustainable water management.

–

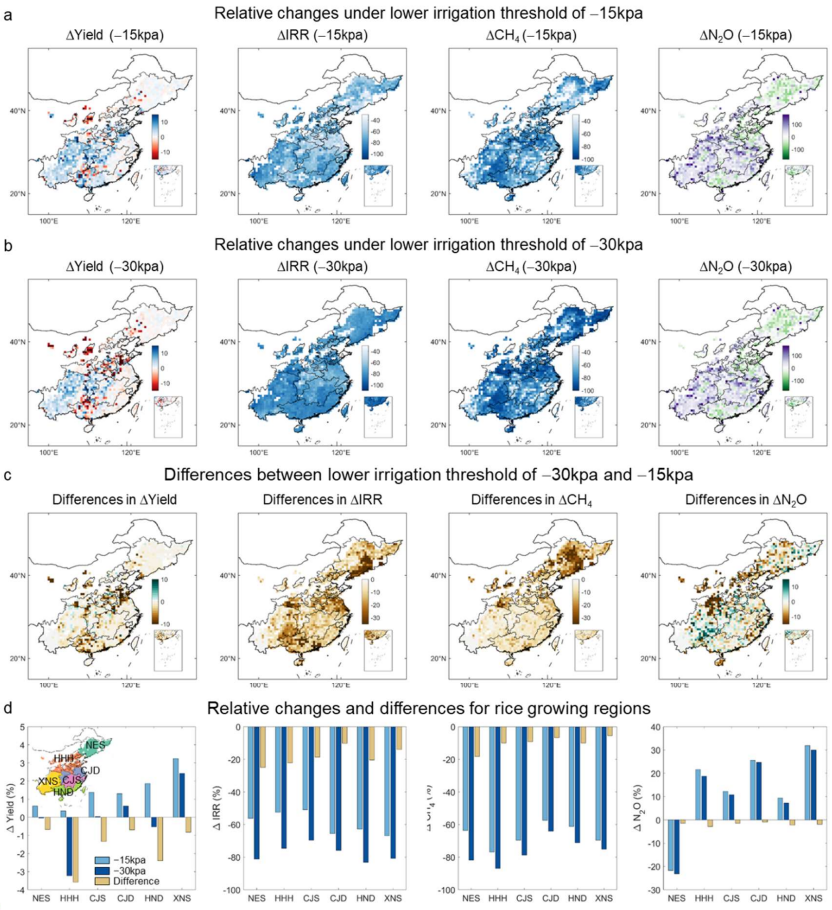

=

Figure 4 Spatial pattern of relative changes in target variables under different irrigation schemes and differences. The four columns correspond to the four target variables ΔYield, ΔIRR, ΔCH_4, and ΔN_2O, respectively. **(a)** relative changes of target variables under a lower irrigation potential of −15 kpa, **(a)** relative changes of target variables under a lower irrigation potential of −30 kpa, **(c)** differences between (b) and (a), **(d)** results for different rice growing regions. NES, HHH, CJS, CJD, HND, and XNS indicate six rice growing areas of China, namely, Northeast Single rice, HuangHuaiHai single rice, Yangtze River single rice, Yangtze River double Rice, South China Double rice, and Southwest China Single rice, respectively.

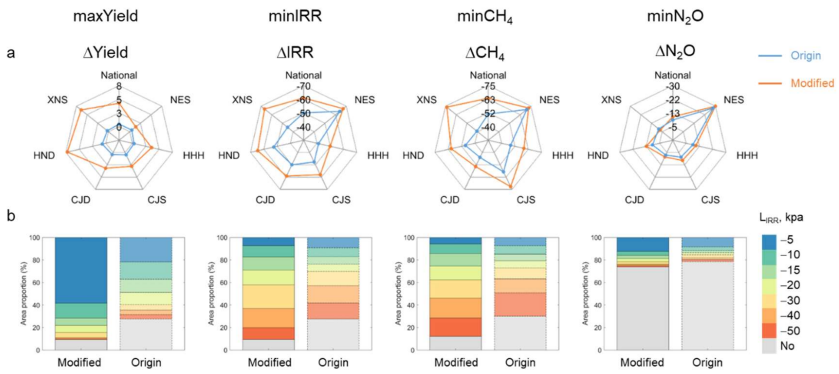

Figure 6~~5~~ Comparison of the origin and modified model from (a) regulation potentials and (b) optimized irrigation schemes under single-objective targets. The four columns show results under four single objective targets: maximizing rice yield (*maxYield*), minimizing irrigation water use (*minIRR*), minimizing CH_4 emissions (*minCH₄*), and minimizing N_2O emissions (*maxN₂O*). **(a)** Area-weighted ΔYield, ΔIRR, ΔCH_4, and ΔN_2O for China and six rice growing regions. Blue and orange indicate results from the origin and modified model, respectively. **(b)** Proportions of rice areas with corresponding optimized lower irrigation thresholds (L_{IRR}) to total irrigated rice areas under the four single objective targets. NES, HHH, CJS, CJD, HND, and XNS indicate six rice growing areas of China, namely, Northeast Single rice, HuangHuaiHai single rice, Yangtze River single rice, Yangtze River double Rice, South China Double rice, and Southwest China Single rice, respectively.

3.4 Tradeoffs between food, water, and greenhouse gas emissions

The NSGA-II algorithm was conducted to investigate synergies or tradeoffs of the food-water-climate nexus (Fig. 6~~-~~7 and Section 2.6). There were evident tradeoffs between reducing CH_4 (or IRR) and N_2O (Fig. 6~~a~~7a). In contrast, synergies were noted between reducing IRR and CH_4, as well as between inhibiting N_2O emissions and increasing rice yield. The relationships between yield increase and CH_4 (or IRR) reductions were more complicated due to the impacts of varying irrigation timing and no-flooded days (Yan et al., 2024). Adopting non-dominated solutions from multi-objective optimization could realize over 90% of the largest reduction potentials of IRR and CH_4, while at the cost of 4% less yield increase (4.6% versus 0.5%) and 25% higher nitrous dioxide emissions (–11% versus 14%). The N_2O increase is because this study used integrated warming potentials of CH_4 and N_2O emissions (GWP) to indicate greenhouse gas emissions so that CH_4 outweighed N_2O due to large emission quantities (Section 2.6).

Spatially, over 90% of the reduction potentials for IRR and CH_4 could be achieved across 53% and 60% of the national rice areas, primarily in southern regions (Fig. 7 and S14). In these areas, N_2O increase was inevitable, but yield increase could be expected.

带格式的: 非上标/ 下标

带格式的: 下标

带格式的: 突出显示

By contrast, stronger tradeoffs occurred in the northern regions, where the reduction potentials of IRR and CH_4 were limited even with decreased yield and increased N_2O emissions. Therefore, NCF adoption should be prioritized in southern regions (e.g., XND, CJD, CJS) to achieve~~Since the multi-objective optimization was conducted targeting~~ a national optimum balance among rice production, water use, and greenhouse gas emissions mitigation~~of food-water-GHGs, NCF practices were adopted in the south regions to realize more considerable IRR and CH_4 reductions contributing to larger national co-benefits~~. Noted that other objective functions could also be designed for multi-objective optimization, such as applying other indicators (e.g., water productivity, yield-scaled GWP), setting distinguished weights for each indicator or grid cell.

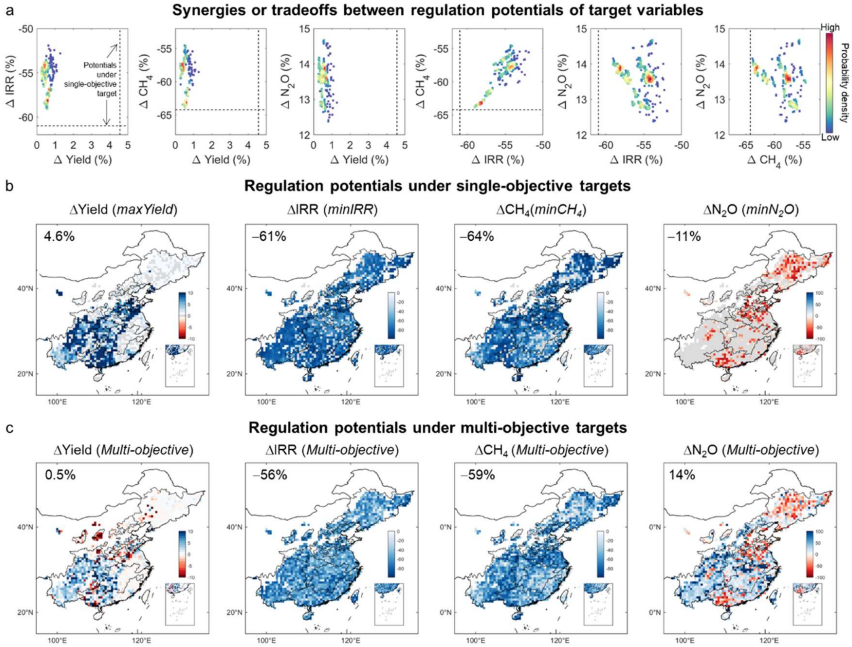

Figure 6~~-~~7 Regulation potentials of ΔYield, ΔIRR, ΔCH_4, and ΔN_2O under single-objective and multi-objective targets. (a) Synergies or tradeoffs between target variables with different solutions of multi-objective optimization. Dots color indicates probability density distributions of variable changes from all non-dominated solutions (N = 10000) of the NSGA II optimization. The vertical and horizontal dashed lines show national regulation potentials of the target variable under single-objective targets, with corresponding spatial distributions presented in panel (b). Note that the results of ΔN_2O potentials (−11%) were not shown in the third, fifth, and sixth subplots for a clearer view. **(b)** ΔYield, ΔIRR, ΔCH_4, and ΔN_2O under single-objective targets of maximizing rice yield (*maxYield*), minimizing irrigation water use (*minIRR*), minimizing CH_4 emissions (*minCH_4*), and minimizing N_2O emissions (*maxN_2O*). These results indicate the maximum benefits of each target variable from

带格式的: 突出显示
带格式的: 突出显示
带格式的: 突出显示
带格式的: 突出显示
带格式的: 突出显示
带格式的: 突出显示
带格式的: 下标, 突出显示
带格式的: 突出显示
带格式的: 突出显示
带格式的: 突出显示
带格式的: 突出显示
带格式的: 突出显示
带格式的: 突出显示
带格式的: 突出显示
带格式的: 突出显示

adopting non-continuous irrigation, which could not be necessarily realized simultaneously. **(c)** ΔYield, ΔIRR, ΔCH_4, and ΔN_2O under multi-objective optimization. These figures show mean benefits from all non-dominated solutions of the NSGA II optimization (N = 10000).

3.5 Uncertainties and future direction

This framework is subject to several uncertainties, mainly sourced from observational gaps and management-related input data. First, the absence of field observations for baseline CH_4 and N_2O emissions across regional scales forced us to use estimates from inventory or data-driven approaches as a proxy for deriving gridded model parameters of this study (Cui et al., 2021; Crippa et al., 2024). Despite uncertainties in predicting absolute values, these parameters could reasonably reproduce the spatial patterns and could be further refined given increased field observations. Second, the limited experimental observations of CH_4 (n = 37) and N_2O (n = 14) under various irrigation schemes have contributed to uncertainties in developing and applying parameter transfer functions (PTFs). The values of PTFs predictors (bulk density and field water capacity) in the observation dataset (1.34~1.48 g cm^{-3} and 0.25~0.30 cm^3 cm^{-3}) did not encompass the full range across national rice areas (1.24~1.48 g $cm^{-3}$and 0.22~0.32 cm^3 cm^{-3}), indicating potential extrapolation in parameters regionalization (Fig. S1). Despite these uncertainties, the PTFs significantly improved over previous approaches (constant parameters or spatial proximity approach). Lastly, current irrigation practices across large scales remain largely unknown, so that irrigation thresholds were set following previous recommendations. However, actual farmer practices are influenced by various factors and may not align with these recommendations. This discrepancy could lead to an overestimation or underestimation of target variables and further introduce uncertainties to the assessment of regulation potentials.

These uncertainties provide insights to enlighten future research efforts, including conducting extensive observations and experiments and developing high-resolution input data. On the one hand, intensive GHGs monitoring networks are essential to reduce uncertainties associated with parametrization (Arenas-Calle et al., 2024). To better constrain the PTFs and reduce extrapolation uncertainty, field experiments combined with incubation experiments ~~covering~~ across a broader range of climate conditions (e.g., colder and more humid areas) and soil properties (e.g., areas with higher SOC or lower bulk density) ~~, including bulk density and field water capacity,~~ should be conducted (Fig. S1). In addition, extensive field experiments with simultaneous measurements of yield, IRR, CH_4, and N_2O emissions across diverse environments are required to validate the framework further. On the other hand, developing a high-resolution dataset of current irrigation schemes is crucial for more accurate model parameter calibration and realistic assessment of regulation potentials. This could be achieved by integrating remote sensing technologies with extensive field investigations (Novick et al., 2022).

带格式的: 字体颜色: 蓝色

带格式的: 突出显示

带格式的: 突出显示

带格式的: 突出显示

带格式的: 突出显示

带格式的: 突出显示

4 Conclusion

This study introduced an advancing framework for process-based modelling of the complex food-water-climate nexus in rice fields under various water management schemes. By integrating the Soil Water Heat Carbon Nitrogen Simulator (WHCNS) with key physiological effects, a novel model upscaling method, and the NSGA-II multi-objective optimization algorithm at a parallel computing platform, the framework provides a comprehensive approach to optimize irrigation strategies. Applying this framework to China's rice cropping system, we assessed the largest regulation potentials of ΔYield, ΔIRR, ΔCH_4, and ΔN_2O as 4.6%, −61.0%, −64.2%, and −10.9% from 91%, 91%, 88%, and 26% of national rice areas. However, these regulation potentials could not be simultaneously realized due to complicated tradeoffs among food-water-GHGs. Based on NSGA II multi-objective optimization targeting food-water-GHGs co-benefits, over 90% of the reduction potentials in water use and methane emissions could be realized, while at the cost of 4% less yield increase and 25% higher nitrous dioxide emissions. The proposed framework is a valuable tool for irrigation optimization in rice cultivation and also offers a transferable paradigm for incorporating other management effects into process-based models, thus supporting comprehensive assessments of sustainable management measures.

Appendix: abbreviation table

Type	Abbreviation	Description
Target variables	*Yield*	R~~r~~ice yield (kg ha^{-1})
	IRR	~~irrigation~~ Irrigation water use (mm)
	CH_4	~~methane~~ Methane emissions (kg ha^{-1})
	N_2O	~~nitrous~~ Nitrous oxide emissions (kg ha^{-1})
	GWP	~~integrated~~ Integrated global warming potential of CH_4 and N_2O at 100-yearr scale, calculated as 27.2×CH_4 +273×N_2O (kg ha^{-1})
	LAI	~~leaf~~ Leaf area index (m^2 m^{-2})
	Pn	~~net~~ Net photosynthetic rate (kg ha^{-1})
	HI	~~harvest~~ Harvest index (-)
Effect sizes	R^{Yield}, R^{IRR}, R^{CH4}, R^{N2O}, R^{LAI}, R^{Pn}, R^{HI}	Effect size of non-continuous flooding irrigation (NCF) on target variables, calculated as the ratio of observations under NCF to that under continuous flooding (CF) (-)
Relative changes	*ΔYield, ΔIRR, ΔCH_4, ΔN_2O*	Relative changes of target variables under NCF compared to CF, calculated as (R-1)×100 (%)
Model parameters	*Cumtemp*	accumulated temperature for crop maturity (◦C)
	AMIN	~~minimum~~ Minimum assimilation rates (kg hm^{-2} h^{-1})
	P^{LAI}, P^{Pn}, P^{HI}	~~genetic~~ Genetic parameters accounting for cultivar sensitivities to NCF effects on leaf area

带格式表格

		index, net photosynthetic rate, and harvest index
	MPmax	~~maximum~~ Maximum CH_4 production rate per soil weight at 30 °C (g C g^{-1} d^{-1})
	f_{N2O_d}	~~maximum~~ Maximum portion of denitrification to N_2O production (-)
Environmental variables	*T*	~~mean~~ Mean daily air temperature during rice growing season (◦C)
	P	~~total~~ Total precipitation during rice growing season (mm)
	PETc	~~total~~ Total crop evapotranspiration during rice growing season (mm)
	CWA	~~climatological~~ Climatological water availability, calculated as the difference between *P* and *PETc* (*P-PETc*, mm)
Soil variables	*BD*	~~bulk~~ Bulk density (g cm^{-3})
	Sand	~~sand~~ Sand content (%)
	Clay	Clay content (%)
	SOC	~~soil~~ Soil organic carbon (%)
	SAT	~~saturated~~ Saturated water content (cm^3 cm^{-3})
	FWC	Ff~~ield~~ water capacity (cm^3 cm^{-3})
Management variables	L_{AWD}	~~lower~~ Lower irrigation threshold, indicated by SWP (kpa)
	U_{AWD}	~~upper~~ Upper irrigation threshold (cm)
	SWP	~~soil~~ Soil water potential (kpa)
	UFR	~~ratio~~ Ratio of unflooded days to total growing days (%)
Optimization objectives	*maxYield*	~~maximizing~~ Maximizing rice yield
	minIRR	~~minimizing~~ Minimizing irrigation water use
	$minCH_4$	~~minimizing~~ Minimizing CH_4 emission
	$minN_2O$	~~minimizing~~ Minimizing N_2O emissions

Code and data availability

The ~~executable~~ origin code of WHCNS model and required model input files are available at https://figshare.com/s/139f3ad8a70faa99724d. Spatial dataset of harvested area of irrigated rice is available from https://doi.org/10.7910/DVN/KAGRFI. Origin c~~C~~limate data is available from~~–~~ https://cds.climate.copernicus.eu/datasets/reanalysis-era5-single-levels?tab=download~~https://cds.climate.copernicuseu/cdsapp#!/search?type=dataset~~. Origin ~~S~~soil data ~~are~~ is available from https://doi.org/10.1002/2013MS000293~~–~~ ~~http://globalchange.bnu.edu.cn/research/data~~. Processed climate and soil data for model running are included in the figshare repository (see Readme for detailed explanations of each file). Crop calendar data are available from ~~–~~ https://zenodo.org/record/5062513. All other data that support the findings of this

study are available in the main text or the Supplementary Information.

Acknowledgements

This study was supported by the National Natural Science Foundation of China (42225102, 42361144876, F.Z.; 42477374, H.L).

带格式的: 突出显示

Author contributions

F.Z. designed the study. Y.B. and H.L. performed all computational analyses. Y.B., H.L. and F.Z. drafted the paper. Y.B., H.L., T. L. and F.Z. reviewed and commented on the manuscript.

Conflict of interest statement

The authors declare no conflicts of interest.

Reference

The world bank. Water resources management. (https://www.worldbank.org/en/topic/waterresourcesmanagement), 2017.

Arenas-Calle, L., Sherpa, S., Rossiter, D., Nayak, H., Urfels, A., Kritee, K., Poonia, S., Singh, D. K., Choudhary, A., Dubey, R., Kumar, V., Nayak, A. K., and McDonald, A.: Hydrologic variability governs GHG emissions in rice-based cropping systems of Eastern India, Agr Water Manage, 301, 108931, https://doi.org/10.1016/j.agwat.2024.108931, 2024.

Balaine, N., Carrijo, D. R., Adviento-Borbe, M. A., and Linquist, B.: Greenhouse Gases from Irrigated Rice Systems under Varying Severity of Alternate-Wetting and Drying Irrigation, Soil Science Society of America Journal, 83, 1533-1541, https://doi.org/10.2136/sssaj2019.04.0113, 2019.

Bo, Y., Jägermeyr, J., Yin, Z., Jiang, Y., Xu, J., Liang, H., and Zhou, F.: Global benefits of non-continuous flooding to reduce greenhouse gases and irrigation water use without rice yield penalty, Global Change Biology, 28, 3636-3650, https://doi.org/10.1111/gcb.16132, 2022.

Bo, Y., Zhou, F., Zhao, J., Liu, J., Liu, J., Ciais, P., Chang, J., and Chen, L.: Additional surface-water deficit to meet global universal water accessibility by 2030, J Clean Prod, 320, 128829, https://doi.org/10.1016/j.jclepro.2021.128829, 2021.

Bouman, B. A. M., Kropff, M., Tuong, T. P., Wopereis, M. C. S., Berge, H. F. M. t., and Laar, H. H. V.: ORYZA2000 : modeling lowland rice,

Carlson, K. M., Gerber, J. S., Mueller, N. D., Herrero, M., MacDonald, G. K., Brauman, K. A., Havlik, P., O'Connell, C. S., Johnson, J. A., Saatchi, S., and West, P. C.: Greenhouse gas emissions intensity of global croplands, Nature Climate Change, 7, 63-68, 10.1038/nclimate3158, 2017.

Carrijo, D. R., Lundy, M. E., and Linquist, B. A.: Rice yields and water use under alternate wetting and drying irrigation: A meta-analysis, Field Crop Res, 203, 173-180, 2017.

Chen, M., Linker, R., Wu, C., Xie, H., Cui, Y., Luo, Y., Lv, X., and Zheng, S.: Multi-objective optimization of rice irrigation modes using ACOP-Rice model and

historical meteorological data, Agr Water Manage, 272, 107823, https://doi.org/10.1016/j.agwat.2022.107823, 2022.
Crippa, M., Guizzardi, D., Pagani, F., Schiavina, M., Melchiorri, M., Pisoni, E., Graziosi, F., Muntean, M., Maes, J., Dijkstra, L., Van Damme, M., Clarisse, L., and Coheur, P.: Insights into the spatial distribution of global, national, and subnational greenhouse gas emissions in the Emissions Database for Global Atmospheric Research (EDGAR v8.0), Earth Syst. Sci. Data, 16, 2811-2830, 10.5194/essd-16-2811-2024, 2024.
Cui, X., Zhou, F., Ciais, P., Davidson, E. A., Tubiello, F. N., Niu, X., Ju, X., Canadell, J. G., Bouwman, A. F., Jackson, R. B., Mueller, N. D., Zheng, X., Kanter, D. R., Tian, H., Adalibieke, W., Bo, Y., Wang, Q., Zhan, X., and Zhu, D.: Global mapping of crop-specific emission factors highlights hotspots of nitrous oxide mitigation, Nature Food, 2, 886-893, 10.1038/s43016-021-00384-9, 2021.
Deb, K., Pratap, A., Agarwal, S., and Meyarivan, T.: A fast and elitist multiobjective genetic algorithm: NSGA-II, IEEE Transactions on Evolutionary Computation, 6, 182-197, 10.1109/4235.996017, 2002.
Doherty, J.: PEST: Model Independent Parameter Estimation, 2010.
Feddes, R. A. and Zaradny, H.: Model for simulating soil-water content considering evapotranspiration — Comments, Journal of Hydrology, 37, 393-397, https://doi.org/10.1016/0022-1694(78)90030-6, 1978.
Flörke, M., Schneider, C., and McDonald, R. I.: Water competition between cities and agriculture driven by climate change and urban growth, Nature Sustainability, 1, 51-58, 10.1038/s41893-017-0006-8, 2018.
Forster, P., T. Storelvmo, Armour, K., Collins, W., Dufresne, J. L., Frame, D., Lunt, D. J., Mauritsen, T., Palmer, M. D., Watanabe, M., Wild, M., and Zhang, H.: The Earth's Energy Budget, Climate Feedbacks, and Climate Sensitivity. In: Climate Change 2021: The Physical Science Basis. Contribution of Working Group I to the Sixth Assessment Report of the Intergovernmental Panel on Climate Change [Masson-Delmotte, V., P. Zhai, A. Pirani, S. L. Connors, C. Péan, S. Berger, N. Caud, Y. Chen, L. Goldfarb, M. I. Gomis, M. Huang, K. Leitzell, E. Lonnoy, J.B.R. Matthews, T. K. Maycock, T. Waterfield, O. Yelekçi, R. Yu and B. Zhou (eds.)]. Cambridge University Press. In Press., 2021.
Guo, D., Olesen, J. E., Manevski, K., and Ma, X.: Optimizing irrigation schedule in a large agricultural region under different hydrologic scenarios, Agr Water Manage, 245, 106575, https://doi.org/10.1016/j.agwat.2020.106575, 2021.
Han, E. I., Amor; Koo, Jawoo "Global High-Resolution Soil Profile Database for Crop Modeling Applications", http://dx.doi.org/10.7910/DVN/1PEEY0, Harvard Dataverse, V1, 2015.
Hersbach, H., Bell, B., Berrisford, P., Biavati, G., Horányi, A., Muñoz Sabater, J., Nicolas, J., Peubey, C., Radu, R., Rozum, I., Schepers, D., Simmons, A., Soci, C., Dee, D., Thépaut, J.-N.: ERA5 hourly data on single levels from 1979 to present. Copernicus Climate Change Service (C3S) Climate Data Store (CDS). (Accessed on < 06-10-2021>), 10.24381/cds.adbb2d47, 2018.
Ishfaq, M., Farooq, M., Zulfiqar, U., Hussain, S., Akbar, N., Nawaz, A., and Anjum, S.

978 A.: Alternate wetting and drying: A water-saving and ecofriendly rice
979 production system, Agr Water Manage, 241, 106363,
980 https://doi.org/10.1016/j.agwat.2020.106363, 2020.
981 Jägermeyr, J., Müller, C., Ruane, A. C., Elliott, J., Balkovic, J., Castillo, O., Faye, B.,
982 Foster, I., Folberth, C., Franke, J. A., Fuchs, K., Guarin, J. R., Heinke, J.,
983 Hoogenboom, G., Iizumi, T., Jain, A. K., Kelly, D., Khabarov, N., Lange, S.,
984 Lin, T.-S., Liu, W., Mialyk, O., Minoli, S., Moyer, E. J., Okada, M., Phillips, M.,
985 Porter, C., Rabin, S. S., Scheer, C., Schneider, J. M., Schyns, J. F., Skalsky, R.,
986 Smerald, A., Stella, T., Stephens, H., Webber, H., Zabel, F., and Rosenzweig, C.:
987 Climate impacts on global agriculture emerge earlier in new generation of
988 climate and crop models, Nature Food, 2, 873-885, 10.1038/s43016-021-00400-
989 y, 2021.
990 Jiang, W., Huang, W., Liang, H., Wu, Y., Shi, X., Fu, J., Wang, Q., Hu, K., Chen, L.,
991 Liu, H., and Zhou, F.: Is rice field a nitrogen source or sink for the environment?,
992 Environmental Pollution, 283, 117122,
993 https://doi.org/10.1016/j.envpol.2021.117122, 2021.
994 Jiang, Y., Carrijo, D., Huang, S., Chen, J., Balaine, N., Zhang, W. J., van Groenigen, K.
995 J., and Linquist, B.: Water management to mitigate the global warming potential
996 of rice systems: A global meta-analysis, Field Crop Res, 234, 47-54, 2019.
997 Kritee, K., Nair, D., Zavala-Araiza, D., Proville, J., Rudek, J., Adhya, T. K., Loecke, T.,
998 Esteves, T., Balireddygari, S., Dava, O., Ram, K., S. R., A., Madasamy, M.,
999 Dokka, R. V., Anandaraj, D., Athiyaman, D., Reddy, M., Ahuja, R., and
1000 Hamburg, S. P.: High nitrous oxide fluxes from rice indicate the need to manage
1001 water for both long- and short-term climate impacts, Proceedings of the
1002 National Academy of Sciences, 115, 9720-9725, doi:10.1073/pnas.1809276115,
1003 2018.
1004 Lampayan, R. M., Rejesus, R. M., Singleton, G. R., and Bouman, B. A. M.: Adoption
1005 and economics of alternate wetting and drying water management for irrigated
1006 lowland rice, Field Crop Res, 170, 95-108, 2015.
1007 Li, T., Angeles, O., Marcaida, M., Manalo, E., Manalili, M. P., Radanielson, A., and
1008 Mohanty, S.: From ORYZA2000 to ORYZA (v3): An improved simulation
1009 model for rice in drought and nitrogen-deficient environments, Agricultural and
1010 Forest Meteorology, 237-238, 246-256,
1011 https://doi.org/10.1016/j.agrformet.2017.02.025, 2017.
1012 Liang, H., Yang, S., Xu, J., and Hu, K.: Modeling water consumption, N fates, and rice
1013 yield for water-saving and conventional rice production systems, Soil and
1014 Tillage Research, 209, 104944, https://doi.org/10.1016/j.still.2021.104944,
1015 2021.
1016 Liang, H., Hu, K., Qi, Z., Xu, J., and Batchelor, W. D.: A distributed agroecosystem
1017 model (RegWHCNS) for water and N management at the regional scale: A case
1018 study in the North China Plain, Computers and Electronics in Agriculture, 213,
1019 108216, https://doi.org/10.1016/j.compag.2023.108216, 2023.
1020 Liang, H., Xu, J., Hou, H., Qi, Z., Yang, S., Li, Y., and Hu, K.: Modeling CH_4 and N_2O
1021 emissions for continuous and noncontinuous flooding rice systems, Agr Syst,

203, 103528, https://doi.org/10.1016/j.agsy.2022.103528, 2022.
Novick, K. A., Ficklin, D. L., Baldocchi, D., Davis, K. J., Ghezzehei, T. A., Konings, A. G., MacBean, N., Raoult, N., Scott, R. L., Shi, Y. N., Sulman, B. N., and Wood, J. D.: Confronting the water potential information gap, Nat Geosci, 15, 158-164, 2022.
Song, H., Zhu, Q. a., Blanchet, J.-P., Chen, Z., Zhang, K., Li, T., Zhou, F., and Peng, C.: Central Role of Nitrogen Fertilizer Relative to Water Management in Determining Direct Nitrous Oxide Emissions From Global Rice - Based Ecosystems, Global Biogeochemical Cycles, 37, 2023.
Tan, J., Zhao, S., Liu, B., Luo, Y., and Cui, Y.: Global sensitivity analysis and uncertainty analysis for drought stress parameters in the ORYZA (v3) model, Agronomy Journal, 113, 1407-1419, https://doi.org/10.1002/agj2.20580, 2021.
Tang, Y., Su, X., Wen, T., McBratney, A. B., Zhou, S., Huang, F., and Zhu, Y.-g.: Soil properties shape the heterogeneity of denitrification and NO emissions across large-scale flooded paddy soils, Global Change Biology, 30, e17176, https://doi.org/10.1111/gcb.17176, 2024.
Tian, Z., Fan, Y. D., Wang, K., Zhong, H. L., Sun, L. X., Fan, D. L., Tubiello, F. N., and Liu, J. G.: Searching for "Win-Win" solutions for food-water-GHG emissions tradeoffs across irrigation regimes of paddy rice in China, Resour Conserv Recy, 166, 2021.
Tsuji, G. Y., Hoogenboom, G., and Thornton, P. K.: Understanding Options for Agricultural Production, Systems Approaches for Sustainable Agricultural Development,
Xu, J. Z., Liao, Q., Yang, S. H., Lv, Y. P., Wei, Q., Li, Y. W., and Hameed, F.: Variability of Parameters of ORYZA (v3) for Rice under Different Water and Nitrogen Treatments and the Cross Treatments Validation, Int J Agric Biol, 20, 221-229, 2018.
Yan, Y., Ryu, Y., Li, B., Dechant, B., Zaheer, S. A., and Kang, M.: A multi-objective optimization approach to simultaneously halve water consumption, CH4, and N2O emissions while maintaining rice yield, Agricultural and Forest Meteorology, 344, 109785, https://doi.org/10.1016/j.agrformet.2023.109785, 2024.
Yang, J. C. and Zhang, J. H.: Crop management techniques to enhance harvest index in rice, J Exp Bot, 61, 3177-3189, 2010.
Yuan, S., Linquist, B. A., Wilson, L. T., Cassman, K. G., Stuart, A. M., Pede, V., Miro, B., Saito, K., Agustiani, N., Aristya, V. E., Krisnadi, L. Y., Zanon, A. J., Heinemann, A. B., Carracelas, G., Subash, N., Brahmanand, P. S., Li, T., Peng, S., and Grassini, P.: Sustainable intensification for a larger global rice bowl, Nature Communications, 12, 7163, 10.1038/s41467-021-27424-z, 2021.
Zhang, B., Tian, H., Ren, W., Tao, B., Lu, C., Yang, J., Banger, K., and Pan, S.: Methane emissions from global rice fields: Magnitude, spatiotemporal patterns, and environmental controls, Global Biogeochemical Cycles, 30, 1246-1263, https://doi.org/10.1002/2016GB005381, 2016.

Zhang, H., Zhang, S., Yang, J., Zhang, J., and Wang, Z.: Postanthesis Moderate Wetting Drying Improves Both Quality and Quantity of Rice Yield, Agronomy Journal, 100, 726-734, https://doi.org/10.2134/agronj2007.0169, 2008.

Zhang, H., Adalibieke, W., Ba, W., Butterbach-Bahl, K., Yu, L., Cai, A., Fu, J., Yu, H., Zhang, W., Huang, W., Jian, Y., Jiang, W., Zhao, Z., Luo, J., Deng, J., and Zhou, F.: Modeling denitrification nitrogen losses in China's rice fields based on multiscale field-experiment constraints, Global Change Biology, 30, e17199, https://doi.org/10.1111/gcb.17199, 2024.

Zhang, Y., Wang, W., Li, S., Zhu, K., Hua, X., Harrison, M. T., Liu, K., Yang, J., Liu, L., and Chen, Y.: Integrated management approaches enabling sustainable rice production under alternate wetting and drying irrigation, Agr Water Manage, 281, 108265, https://doi.org/10.1016/j.agwat.2023.108265, 2023.